The Orthotropic Elastic Constants and Vibrational Modes of Plywood Plates by Experiment and Finite Element Analysis

John Coffey, Cheshire, UK.

November 2012

Key words: orthotropic, elastic constant determination, birch plywood, finite element, Strand7 FEA program, resonant modes and frequencies, Chladni figures, FEA compared with experiment.

1 Topics addressed

This article is a successor to one entitled 'Modelling an Orthotropic Material by an Assemblage of Isotropic Components'by the present author, also published on the MathStudio.co.uk website. The overall context is my interest in the acoustics of the violin and viola. As part of this I have been looking into the vibration of thin (3 to 4 mm) plywood plates and attempting to quantify resonant behaviour by both experiments and finite element models. The experiments to date have involved measuring Young's modulus and shear moduli in static tests, and in measuring the resonant frequencies and Chladni figure nodal patterns of transverse vibration of specimen plates. For the previous article the finite element model used was the LISA 7 program. However, because LISA 7 did not accommodate orthotropic materials, orthotropic behaviour was simulated by means of an assemblage of 3D elastically isotropic brick elements. For this current investigation I have been able to use the Strand7 program, version 2.4.4, which does provide static and dynamic modelling with orthotropic 2D plate-shell elements.

Wood and plywood are orthotropic, meaning that their elastic constants are different in the three principle directions of along, across and through the grain. For bulk material there are nine independent elastic constants:

- three Young's moduli: E_1 along the grain (surface grain for plywood), E_2 across the grain, and E_3 through the thickness of plywood, or in the radial direction of tree growth for solid wood.
- three shear moduli : G_{12} for in-plane shear, acting to shear the ply laminates across each other, G_{23} and G_{31} for shear through the thickness,
- three corresponding Poisson's ratios, ν_{12} (in-plane), ν_{23} and ν_{31}.

Though E_1 and E_2 can be measured quite readily by static bending of strip specimens, and G_{23} and G_{31} measured by twisting, the other constants are not readily determined. In thin materials, however, where there is negligible shear through the thickness, E_3, ν_{23} and ν_{31} have little effect. In the previous article I did consider whether most elastic constants could be determined by matching a FEA model on normal modes of vibration with those measured experimentally.

In this present article I investigate these related topics:

1. a method using resonant frequencies for determining the dominant elastic constants of orthortropic sheet materials,

2. the effect of each of the main elastic constants, varied one at a time, on the resonant frequencies,

3. the effect on nodal patterns (lines over the plate surface of almost zero transverse displacement) of changing the direction of the wood grain with respect to the geometrical edges of the rectangular plates,

4. whether a consistent set of elastic parameters can be input to the Strand7 FEA program to give a close match to the experimental observations. Such a match would encourage the view that the orthotropic constants of that particular type of plywood had thus been determined.

2 Experimental study

The experimental technique has been essentially the same as that described in the previous article. The study has been of free, unconstrained plates. Briefly, each plate specimen was held fairly near a microphone and tapped with the knuckle a few times in different places. The acoustic spectra of several tap sounds were obtained using the Japanese WaveSpectra program and the frequencies of the main peaks recorded. The dominant peaks, and those which appear in almost all tap spectra, indicate resonant modes. Chladni figures were then determined for that plate. The plate was placed horizontally over a loudspeaker unit or electromagnetic acoustic exciter and driven from an oscillator at and near each resonant frequency in turn. Fine dust particles sprinkled over the plate soon migrate over the surface under the vibrational excitation and accumulate where transverse velocity (normal to the plate) is almost zero. The patterns of node lines were photographed as shown in the sections below.

The only significant difference in technique from that used for the previous article has been the acquisition of a 20W acoustic exciter. This is essentially a loudspeaker coil unit without the cone and frame. The unit I bought had two narrow concentric metal annuli, the outer one fixed, the inner one vibrating. Using adhesive I fastened a 36 mm diameter circular disc of balsa wood to the inner annulus to cap it over. This balsa cap was gently domed so that excitation of a plywood plate resting horizontally on the exciter was only at the centre of the dome. The ability to position the excitation of the plate finely within a selected antinode, even when the nodal pattern is complex, has been a useful improvement.

A comment is appropriate about the confidence and accuracy with which the modes can be determined. The WaveSpectra program offers a choice of window function on the times series. Most spectra were examined 8192 sample points at a time with the Hanning window. Other window functions give a more or less smoothed version of a spectrum, but the positions of the peaks have been consistent to within 1 or 2 Hz. A single, strong, isolated peak in one tap tone spectrum can be measured to within 1 Hz, but where peaks are weak or bunched together, precision cannot be more than about 3 Hz. That is why it is necessary to examine at least four tap tones recorded with the plate held and tapped in different places. Some peaks are repeated consistently in all taps spectra, but others are more vague, appearing to drift by 5 Hz and more from one tap to the next.

When it comes to Chladni figures, an important test is to move the acoustic exciter under the specimen to check that the pattern is stable. Where two or more normal modes have close frequencies, the Chladni figure will change when the point of excitation is moved, as the dust particles migrate from one mode to another. A striking example of this is shown in Figure 1, for the specially

orthotropic birch plate at 1300 Hz. The small circle marks the position of the exciter. One half of the plate is in a $(7-n)$ mode and the other in a $(5-n)$ mode. Further confusion can arise where one or more frequency spectra show peaks for which a stable Chladni figure cannot be found. I have taken all reasonable care to confirm the resonant frequencies and nodal patterns, though the study in §3 provides examples where the theory has prompted a re-measurement.

Four specimens of plywood have been measured:

1. birch ply rectangle, 250mm along grain, 300mm across grain, thickness $3 \cdot 65$mm. This was all-birch 3 ply, density 700 kg/m^2.
2. birch ply rectangle, also 250×300mm, but with the grain at 45^o to the edges of the plate.
3. 'red hardwood ply' 250 mm along grain, 300mm across grain, mean thickness $2 \cdot 91$mm. This was a general purpose building ply faced with an unspecified hardwood, density 590 kg/m^2. In fact the face grain was not exactly parallel to the edges of the parent plywood sheet, but about 7^o off.
4. red hardwood ply 240 mm square with the grain nominally at 45^o to the plate edges, but in reality at 52^o.

In this draft report only the birch Specimens 1 and 2 are described.

Figures 2, 3 and 4, and Table 1 respectively give the normal modes for Specimen 1, which is in the special orthotropic orientation (grain parallel to rectangle's edges). The nomenclature is $(m-n)$ where m counts the number of node lines parallel to the grain and n the number across. Modes marked with an asterisk were clear and strong, so are ones for which I feel that the accuracy of frequency is particularly good.

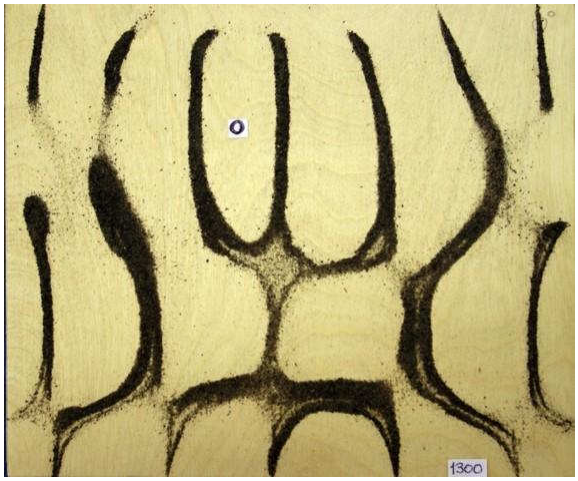

Figure 1: A mixed mode excitation of the birch plywood plate, 250mm by 300 mm, at 1300 Hz. The surface grain runs vertically (y direction) in the picture.

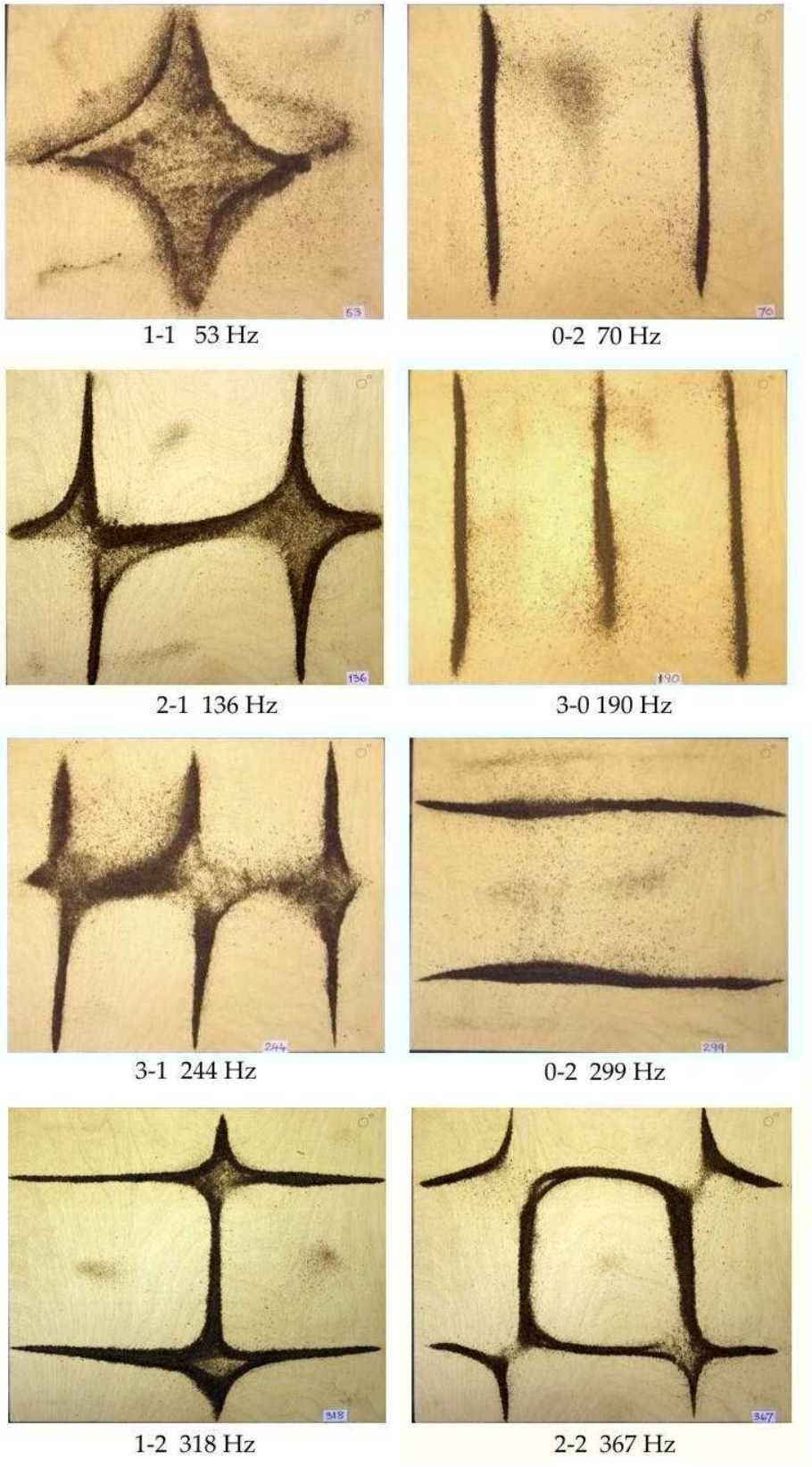

Figure 2: Chladni figures of the low frequency modes of birch 3-ply rectangle, $250 \times 300 \times 3 \cdot 65$ mm. The surface grain is vertical in the photographs.

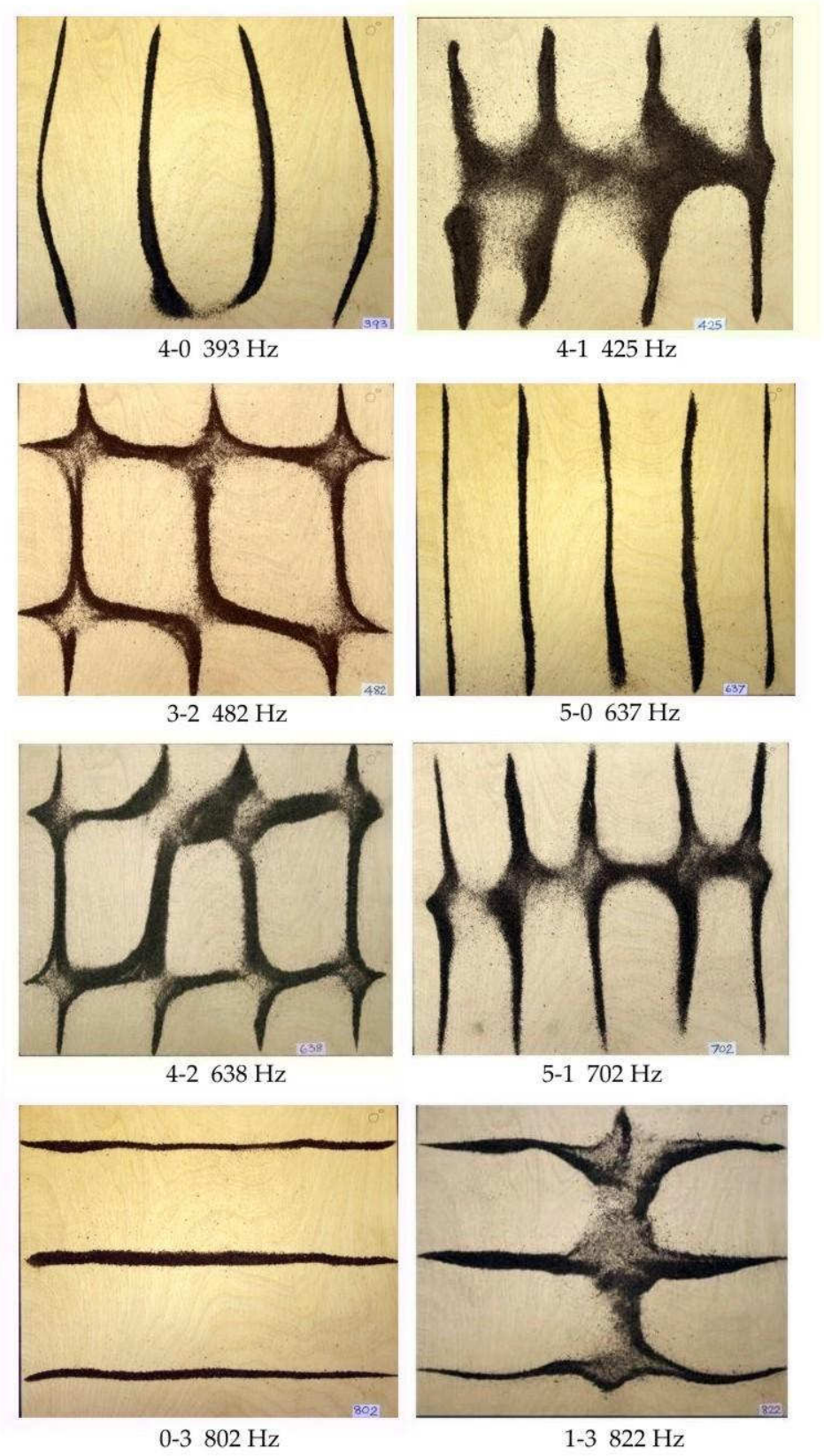

Figure 3: Chladni figures of the mid-frequency modes of same birch 3-ply rectangle.

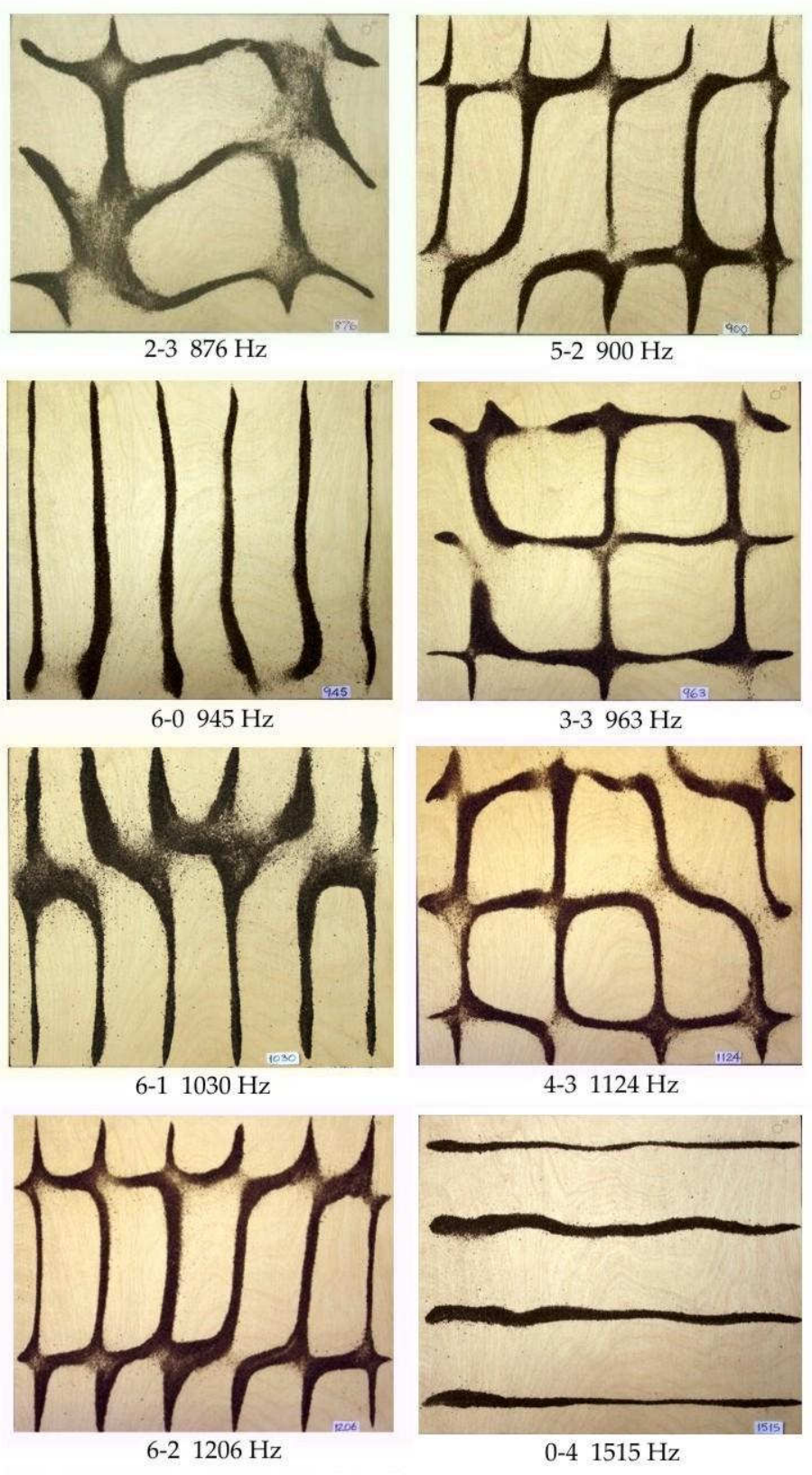

Figure 4: Chladni figures of the high frequency modes of same birch 3-ply rectangle.

Mode	Hz	Mode	Hz
1-1	53	4-2	638
2-0	70	5-1	702
2-1	136	**0-3**	**802**
3-0	**190**	1-3	822
3-1	244	2-3	876
0-2	**299**	5-2	900
1-2	318	6-0	945
2-2	**367**	3-3	963
4-0	393	6-1	1030
4-1	425	**4-3**	**1124**
3-2	482	6-2	1202
5-0	637	0-4	1515

Table 1: Experimentally determined resonant frequencies of 3-ply all-birch rectangle, 250 mm along grain, 300 mm across, 3·65 mm thick. The modes marked in **bold** face were well defined in frequency.

3 Effect of varying individual elastic constants

This section describes a FEA study of the effects of varying the Young's moduli, shear moduli and Poisson's ratios one at a time on the frequencies of the normal modes as predicted by Srand7 – there is no experimental corroboration for these predictions. I have modelled a rectangular plate free of all constraints. Like LISA 7, Strand7 can cope with this indeterminacy, so the first six modes correspond to body translations and rotations without distortion – these are ignored.

The starting point has been published values of the elastic constants for birch plywood, used as input to model the vibration of Specimens 1 and 2 above. I have consulted two sets of data:

- Handbook of Finnish Plywood. Published on line by UPM, Finland. Tables 3-2 and 3-7.
- AS Latvijas Finieris Plywood handbook. Tables 4.9, 2.11, 4.12 (sanded) for Riga ply 4mm.

The values they give are listed in Table 2. Those in the bottom line are close to the average; these have been taken as central reference values for the sets of calculations. I have set E_3 to 500 MPa, ν_{12} to $0 \cdot 2$ and the other two Poisson's ratios to $0 \cdot 3$.

Source	E_1	E_2	G_{12}	G_{23}	G_{31}
UPM Finland	16471	1029	620	≈ 100	169
AS Latvijas Finieris	16941	1059	750	≈ 100	155
Central values used	16700	1045	685	100	160

Table 2: Elastic constants of birch 3-ply, 4mm nominal thickness, in MPa.

The plate elements in the finite element model were 1 cm squares, quad9 type. For the modes above about 900 Hz a refined mesh was used to confirm vibrational patterns, but this refinement did not alter the resonant frequencies. The modal patterns of displacement appeared very similar to the experimental Chladni figures. The fact that plate/shell elements are used means that three of the elastic constants, related to through-thickness stiffness, have no effect on the deformation. These are E_3, ν_{23} and ν_{31}. In Strand7 the quad8 and quad9 elements are 'thick plate' elements, modelling the Mindlin-Reissner approximation. For these the through-thickness shear moduli G_{23} and G_{31} have

an effect, but this is small when the plates are thin, as in our case. So of the 9 independent elastic constants we can expect only E_1, E_2 and G_{12} to have a significant effect.

I have assessed the effect of the six significant elastic constants by varying each in turn about the central values stated above. The resonant frequencies of this central set of data were taken as the references for comparison. I made a large ($> \pm 30\%$) change to each constant in turn, and calculated

$$\frac{\text{maximum frequency - minimum frequency}}{\text{reference frequency}} \%$$

for each mode. Assessing the change relative to the modal frequency is appropriate because pitch is perceived logarithmically. Before looking at some specific cases, consider Table 3 which gives a qualitative summary. As we might expect, changes in E_1 have no effect on modes where the nodal line are parallel to the grain – type $(m-0)$, since all bending is across the grain. However, in addition E_1 has no effect when there is one line across the grain – type $(m-1)$. The greater effect of E_1 is felt in modes $m = 0, 1, 2, \ldots$, the strength dying as m increases. E_2 has complementary effects with the roles of m and n interchanged.

Elastic constant	Significance	Size of % change			
		Zero	Weak	Moderate	Strong
E_1	strong	$n = 0, 1$		high m & $n >= 2$	low m & $n \geq 2$
E_2	strong	$m = 0, 1$		$n \geq 3$	$n = 0, 1$ or m high
E_3	none	-		-	-
G_{12}	moderate	$m = 0$ or $n = 0$		high m, high n	both m & n low
G_{23}	weak		all cases		
G_{31}	weak	$n = 0$	$n = 1, 2$	$n \geq 3$	
ν_{12}	weak		all cases		
ν_{23}	none	-		-	-
ν_{31}	none	-		-	-

Table 3: Qualitative summary of significance of each of the nine elastic constants in modelling an orthotropic plate by quad9 plate-shell elements. Plywood rectangle is 250 mm along grain, 300 mm across and $3 \cdot 65$ mm thick.

Tables 4 to 9 list the percentage changes in resonant frequencies as E_1, E_2, G_{12}, G_{31}, G_{23} and ν_{12} respectively are changed by large amounts. Comparisons within any one table are quantitative. Although tables cannot be compared directly with each other, they do indicate qualitatively the relative significance of the various constants. Note that in every case an increase in the elastic constant causes an increase in frequency. The effects of G_{23} and G_{31} will be larger in thicker specimens.

E_1 : % frequency change				
n	0	1	2	3
m				
0			21	19
1		0	18	19
2	0	0	14	17
3	0	0	9	14
4	0	0	5	11
5	0	0	3	8
6	0	0	2	
7	0	0	1	
8	0			

Table 4: Percentages increase in resonant frequencies as E_1 increases from 13 to 20 GPa, relative to frequencies for $E_1 = 16 \cdot 7$ GPa.

G_{12} : % frequency change				
n	0	1	2	3
m				
0			0	0
1		52	5	1
2	0	40	15	5
3	0	26	22	10
4	0	16	23	15
5	0	10	21	17
6	0	7	17	
7	0	5	14	
8	0			

Table 6: % increase as G_{12} increases from $0{\cdot}3$ to $1 \cdot 0$ GPa.

G_{23} : % frequency change				
n	0	1	2	3
m				
0			0	0
1		$0{\cdot}8$	$0{\cdot}2$	$0{\cdot}1$
2	$0{\cdot}1$	$0{\cdot}8$	$0{\cdot}6$	$0{\cdot}{\cdot}3$
3	$0{\cdot}5$	$0{\cdot}9$	$1{\cdot}0$	$0{\cdot}7$
4	$1{\cdot}1$	$1{\cdot}3$	$1{\cdot}5$	$1{\cdot}2$
5	$1{\cdot}9$	$2{\cdot}0$	$2{\cdot}1$	$1{\cdot}8$
6	$2{\cdot}9$	$2{\cdot}9$	$3{\cdot}0$	
7	$4{\cdot}1$	$4{\cdot}0$	$4{\cdot}0$	
8	$5{\cdot}3$			

Table 8: % increase as G_{23} changes from $0{\cdot}05$ to $0 \cdot 2$ GPa.

E_2 : % frequency change				
n	0	1	2	3
m				
0			0	0
1		2	0	0
2	40	9	2	1
3	40	19	5	2
4	40	26	10	3
5	39	30	15	3
6	39	32	20	
7	38	34	23	
8	35			

Table 5: % increase as E_2 increases from $0 \cdot 6$ to $1 \cdot 4$ GPa.

G_{31} : % frequency change				
n	0	1	2	3
m				
0			$2{\cdot}7$	$9{\cdot}5$
1		$0{\cdot}3$	$2{\cdot}8$	$9{\cdot}2$
2	0	$0{\cdot}8$	$3{\cdot}0$	$9{\cdot}1$
3	0	$1{\cdot}0$	$3{\cdot}1$	$9{\cdot}0$
4	0	$0{\cdot}9$	$3{\cdot}3$	$8{\cdot}7$
5	0	$0{\cdot}8$	$3{\cdot}2$	$8{\cdot}3$
6	0	$0{\cdot}5$	$2{\cdot}9$	
7	0	$0{\cdot}6$	$2{\cdot}6$	
8	0			

Table 7: % increase as G_{31} changes from $0{\cdot}06$ to $0 \cdot 3$ GPa.

ν_{12} : % frequency change				
n	0	1	2	3
m				
0			$2{\cdot}1$	$1{\cdot}4$
1		$0{\cdot}1$	$1{\cdot}2$	$1{\cdot}2$
2	$0{\cdot}1$	$0{\cdot}5$	$2{\cdot}2$	$2{\cdot}0$
3	$0{\cdot}2$	$0{\cdot}9$	$1{\cdot}5$	$2{\cdot}3$
4	$0{\cdot}6$	$1{\cdot}0$	$2{\cdot}9$	$3{\cdot}2$
5	$2{\cdot}1$	$1{\cdot}1$	$3{\cdot}1$	$3{\cdot}7$
6	$1{\cdot}0$	$0{\cdot}7$	$3{\cdot}0$	
7	$1{\cdot}0$	$1{\cdot}5$	$2{\cdot}8$	
8	$0{\cdot}9$			

Table 9: % increase as ν_{12} changes from 0 to $0 \cdot 7$.

4 Fitting elastic constant to resonant frequencies

Since we have a rectangular plate of orthotropic 3-ply birch and have determined its normal modes, can we use this knowledge to determine a set of elastic constants to input into a FEA model so that there is close agreement between theory and experiment? The following approach seems to work fairly well.

Step 1 : Noting that modes $(0-n)$ depend almost entirely on E_1, determine the value of E_1 which brings these frequencies into agreement. For the birch in Table 1, we have experimental values for three of these: (0-2), (0-3) and (0-4), but, for a reasonable mesh size, Strand7 converges only for modes less than about 1400 Hz so (0-4) is not modelled. Table 10 below gives the frequencies of these modes for various values of E_1, all other elastic constants being at their reference values. (These values were the ones used in constructing the percentage tables, Tables 4 to 9.) Interpolation gives $E_1 = 17 \cdot 8$ GPa for (0-2) and $18 \cdot 2$ for (0-3). These is fair agreement so take $E_1 = 18 \cdot 0$ GPa as a working value.

Mode	Expt	13 GPa	$16 \cdot 7$ GPa	20 GPa
0-2	299	256	290	316
0-3	802	687	771	835

Table 10: Frequencies of modes (0-2) and (0-3) in hertz, obtained by experiment and predicted by Strand7 for three values of E_1.

Step 2 : Similarly, a fair value of E_2 can be estimated by interpolation of Table 11 where the fit is to five modes, (2-0) to (6-0). The curve through the four data points has to be extrapolated to higher E_2. This is imprecise; I have used both quadratic and cubic fit and the values given in the right-most column of Table 11 are a rough average, where both give plausible values. I have taken $2 \cdot 05$ GPa as a working value.

Mode	Expt	$0 \cdot 6$ GPa	$0 \cdot 8$ GPa	$1 \cdot 045$ GPa	$1 \cdot 4$ GPa	Interpolated
2-0	70	39	45	51	59	$\approx 2 \cdot 0$
3-0	190	106	123	140	162	$\approx 2 \cdot 0$
4-0	393	208	239	273	316	$\approx 2 \cdot 2$
5-0	637	342	394	450	518	$2 \cdot 15$
6-0	945	509	586	667	767	$2 \cdot 06$

Table 11: Frequencies of modes (2-0) to (6-0) obtained by experiment and predicted by Strand7 for four values of E_2. The corresponding extrapolated value of E_2 to obtain the experimental frequency is listed in the last column.

Step 3 : Mode (1-1) is the only one determined almost entirely by G_{12}. (2-1) is most strongly influenced by G_{12}, but E_2 also has a moderate effect. Hence obtain an estimate by fitting to (1-1) and check against (2-1). Refer to Table 12 where the interpolated values are shown in the right column. Note that if (1-1) were at 54 Hz instead of 53, the implied value of G_{12} would be $0 \cdot 82$ GPa. I take a working value of $G_{12} = 0.9$ GPa.

Leaving the other elastic constants at their reference values, Strand7 has been run with these estimated values of E_1, E_2 and G_{12}. I refined the mesh to obtain convergence at the highest

Mode	Expt	0·3 GPa	0·685 GPa	1·0 GPa	Interpolated
1-1	53	34	50	59	0.79
2-1	136	85	113	130	1.13

Table 12: Frequencies of modes (1-1) and (2-1) obtained by experiment and predicted by Strand7 for three values of G_{12}.

frequencies. The results are listed in Table 13, compared with the experimental results. As in the previous article, a measure Q of quality of fit has been defined by

$$Q = \sum_{modes} \left(\frac{f_{FEA}}{f_{expt}} - 1 \right)^2 \times 1000 :$$

that is, the sum of squared fractional errors in the frequency, f. Its value for this set of input elastic constants is $28 \cdot 4$.

The percentage differences in Table 13 are also presented in Table 14 in the same $(m - n)$ format of Tables 4 to 9 in order to suggest where small adjustments to the assumed elastic constants might be made to improve the fit. Some judgment is needed, but we can see from Table 8 that increasing G_{23} would offset the drift to negative percentage differences for modes $(m - 0)$. However, since (2-0) and (3-0) are already slightly high, a small decrease in E_2 is also indicated. Also G_{12} could be reduced.

Rather than just make a trial-and-error search, I have used the Solve function on the Excel spreadsheet to minimise, in the least squares sense, the aggregated percentage differences by means of adjusting the elastic constants. The method has involved determining a linear combination of the percentages in Tables 4 to 9 that closely matches the percentages in Table 14, mode by mode. One way to look at this is to say that if the values in these tables are regarded as defining surfaces over m, n, then the shape of surface in Table 14 is being modelled by a weighted linear sum of the surfaces in Tables 4 to 9. The Solver facility determines the weights of each Table, 4 to 9, which gives the least squares fit. The final step is to convert these weighting coefficients to revised values of the six elastic constants represented in Tables 4 to 9. The span of each variable is given in the table's caption; a weighting of 1 would correspond to a change by this full amount. The weightings calculated in Solver indicate a *pro rata* change. The only elaboration of this approach has been to weight those modes in Table 1 marked in bold twice as heavily as the other modes on account of the greater confidence in their frequencies. Table 15 lists the initial values of the six elastic constants, the span of each in Tables 4 to 9, the weighting determined by the spreadsheet Solver, and the consequential revised elastic constants. Notice how Poisson's ratio has been pushed to zero.

I have made a second run with Strand7 using the new values in Table 15, and the results are listed in Table 16. Clearly one could finesse the results by further adjustments in the elastic constants, but I consider the agreement to be most satisfactory. I have gone back to check experimentally mode 6-1, which has the largest error, but find that 1030 Hz seems correct. The table explains why modes (5-3) and (7-0) could not be found experimentally – they are extremely close in frequency. In fact, the mixed modes in Figure 1 are these two. Probably some small inhomogeneity in the plywood has caused the top half of the plate to respond in one mode and the lower half in the other.

The FEA-experimental comparison of Table 16 is the main result of this section. We may conclude that, as far as this mode-matching technique is valid, the elastic constants of this type of

Mode	Strand7 Hz	Expt Hz	Diff Hz	Diff %	Quality Q
1–1	57	53	4	7·2	6·0
2–0	71	70	1	1·7	0·3
2–1	136	136	0	−0·1	0·0
3–0	195	190	5	2·7	0·8
3–1	260	244	16	6·0	4·1
0–2	300	299	1	0·5	0·0
1–2	321	318	3	0·8	0·1
2–2	386	367	19	4·9	2·7
4–0	377	393	−16	−4·1	1·6
4–1	440	425	16	3·4	1·2
3–2	493	482	11	2·3	0·5
5–0	622	637	−15	−2·4	0·5
4–2	657	638	19	2·9	0·9
5–1	677	702	−25	−3·7	1·2
0–3	798	802	−4	−0·6	0·0
1–3	813	822	−9	−1·1	0·1
2–3	862	876	−14	−1·6	0·2
5–2	878	900	−22	−2·5	0·6
6–0	917	945	−28	−3·0	0·9
3–3	953	963	−10	−1·1	0·1
6–1	969	1030	−61	−6·2	3·5
4–3	1090	1124	−34	−3·1	0·9
6–2	1154	1202	−48	−4·2	1·6
7–0	1261				
5–3	1278				
7–1	1312				
7–2	1479				
0–4	1481	1515	−34	−2·3	
1–4	1496				**28·4**
6–3	1523				
2–4	1535				
3–4	1610				

Table 13: Resonant frequencies of birch 3-ply plate, Specimen 1, as measured experimentally and predicted by Strand7 with $E_1 = 18 \cdot 0$, $E_2 = 2 \cdot 05$, $G_{12} = 0 \cdot 9$, $G_{23} = 0 \cdot 10$, $G_{31} = 0 \cdot 16$ GPa, $\nu_{12} = 0 \cdot 2$.

3-ply birch is as the bottom row in Table 14, namely

$$E_1 = 17 \cdot 9, \quad E_2 = 2 \cdot 00, \quad G_{12} = 0 \cdot 78, \quad G_{23} = 0 \cdot 50, \quad G_{31} = 0 \cdot 24 \ \text{GPa} \tag{1}$$

and ν_{12} is virtually zero. Of course the values of G_{23}, G_{31} and ν_{12} will be rather tentative since their effects of plates so thin as this are small. Also E_3 cannot be determined at all by finite plate elements.

% diff	n				
m	0	1	2	3	4
0			0·5	−0·6	−2·3
1		7·2	0·8	−1·1	
2	1·7	−0·1	4·9	−1·6	
3	2·7	6·0	2·3	−1·1	
4	−4·1	3·4	2·9	−3·1	
5	−2·4	−3·7	−2·5		
6	−3·0	−6·2	−4·2		

Table 14: Percentage differences in measured and predicted resonant frequencies, from data in Table 13.

	E_1	E_2	G_{12}	G_{23}	G_{31}	ν_{12}
Span	0·7	0·8	0·7	0·15	0·24	0·7
Initial	18	2·05	0·99	0·1	0·16	0·2
Weight	0·102	0·060	0·170	−2·666	−0·342	0·285
New	17·93	2·002	0·781	0·500	0·242	0·0

Table 15: Adjustment of the six elastic constants to give a least squares best fit to values in Table 1. Values are in GPa.

Mode	Strand7 Hz	Expt Hz	Diff Hz	Diff %	Quality Q
1-1	54	53	1	1·5	0·2
2-0	70	70	0	0·7	0·0
2-1	130	136	−6	−4·7	2·0
3-0	194	190	4	2·1	0·5
3-1	252	245	7	2·9	0·9
0-2	301	299	2	0·6	0·0
1-2	319	318	1	0·2	0·0
2-2	375	367	8	2·3	0·5
4-0	380	393	−13	−3·5	1·1
4-1	434	425	9	2·0	0·4
3-2	480	482	−2	−0·4	0·0
5-0	627	637	−10	−1·7	0·3
4-2	642	638	4	0·6	0·0
5-1	677	702	−25	−3·8	1·3
0-3	809	802	7	0·8	0·1
1-3	822	822	0	0·0	0·0
2-3	867	876	−9	−1·1	0·1
5-2	866	900	−34	−4·0	1·5
6-0	934	945	−11	−1·2	0·1
3-3	949	963	−14	−1·4	0·2
6-1	980	1030	−50	−5·1	2·3
4-3	1081	1124	−43	−4·0	1·5
6-2	1153	1202	−49	−4·2	1·6
5-3	1270				
7-0	1300				
7-1	1344				
7-2	1503				
6-3	1522				
0-4	1527	1515	12	0·8	0·1
1-4	1538				**14·9**
2-4	1575				
3-4	1643				

Table 16: Improved fit of resonant frequencies predicted by Strand7 to experimental values, using adjusted elastic constants in last row of Table 15. The quality metric, Q, (in bold) has decreased from over 28 to about 15.

5 Validation on birch 3-ply with grain at 45°

Having determined a consistent set of elastic constants on the free 250×300mm, $3 \cdot 65$ mm thick birch 3-ply plate, this set will now be applied to predict the normal modes of a geometrically identical plate but with the grain at 45 degrees to the plate edges. One can regard the specially orthotropic specimen of §4 as a training data set, and this 45° plate as a validation set. Agreement between FEA and experiment on this specimen will be confirmation both that the Strand7 program closely models reality, and that the procedure for determining the elastic constants is fairly sound.

Orienting the wood grain at 45° to the plate edges is achieved within Strand7 by changing the local axes of all the plate-shell elements. The geometry of the specimen itself is referenced to a global (x, y, z) co-ordinate system such that the longer edge is in the horizontal, x direction. The elastic constants of the plate elements are also defined (within Plate Properties) in the same global co-ordinates, with E_1 parallel to x, E_2 parallel to y, and z in the through-thickness direction. The relation of the local axes of the plates to the global axes is defined by a rotation transformation which the user specifies. For the specially orthotropic plate analysed in the previous section, the local axes of all elements were set at 90^o, to place the grain vertically, as in Figures 2, 3 and 4. For the plate assessed in this present section all local axes were set at 135° to give a grain running NW-SE in the pictures.

For this calculation the mesh of quad9 elements was refined to 12000 in all, each a $2 \cdot 5$mm square. This generous subdivision was merely to ensure convergence of the first 31 modes. A comparison of the first 20 of these with experiment is presented in the matched screen images and photographs of Figures 5 to 8. The Strand7 images are contours of display total displacement in which with zero displacement is the dark blue, yellow-green is half-range and red-pink is maximum displacement. Hence the blue lines correspond with the dust patches of the experimental Chladni figures. The scale is arbitrary and comparison of non-zero displacement amplitudes with experiment is not possible – to do so would require a calculation of dynamic response to a specified excitation.

All first 20 modes are shown in Figures 5 to 8 and all but the two at 618 Hz and 1014 Hz have been found experimentally. About 15 modes were found experimentally as Chladni figures from the tap tones alone, before the finite element calculation was run. The others were found after the calculation, through a search specifically for them. This was necessary because some modes were weak and/or very close in frequency to others. Figure 9 shows two even higher modes for which theory and experiment agree quite well. Above about 1 kHz, however, is it difficult to pick out distinct modes experimentally, and by this time I judged that sufficient confirmation of the finite element model had been attained.

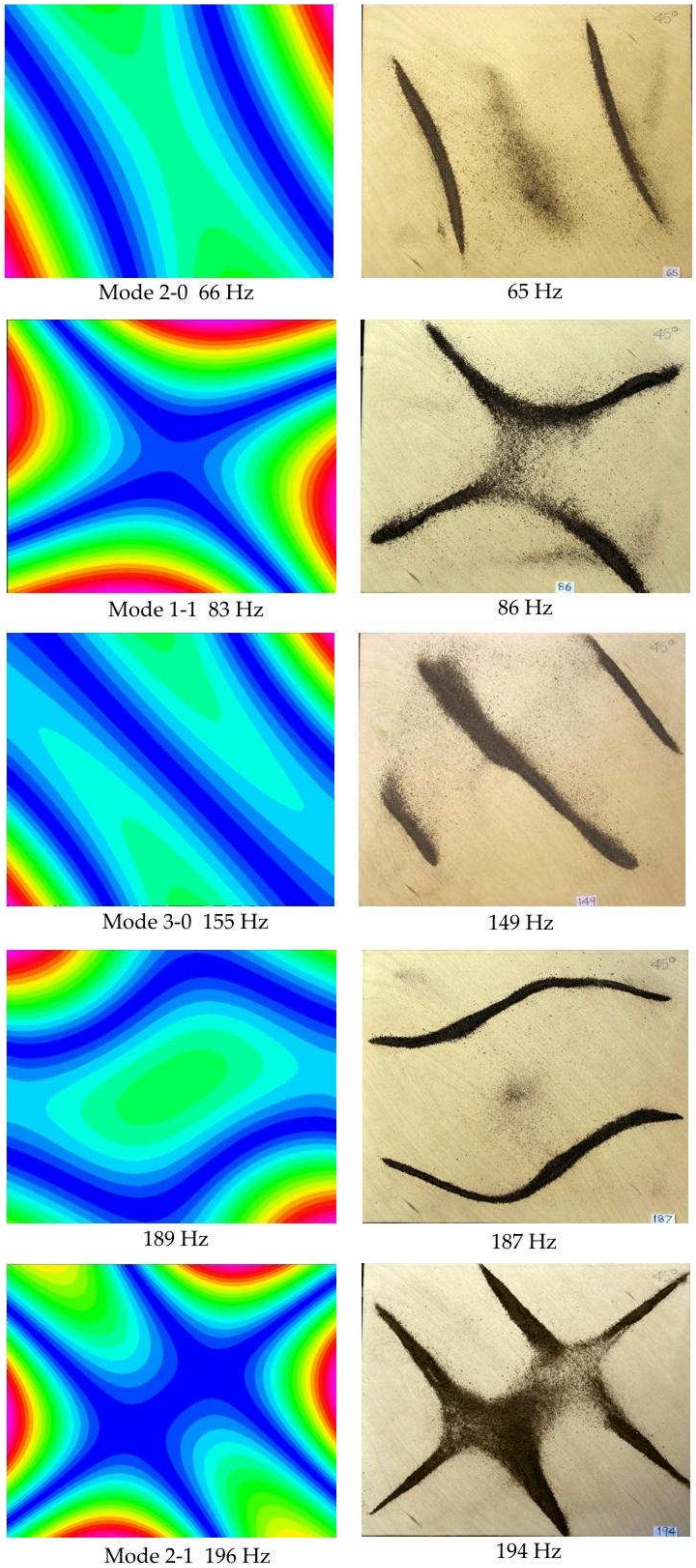

Figure 5: Birch 3-ply with grain at 45 ° to plate edges. Comparison of low frequency modes as predicted by Strand7 with experimental Chladni figures for plate 250mm by 300 mm, $3 \cdot 65$ mm thick. The royal blue contours denote zero displacement.

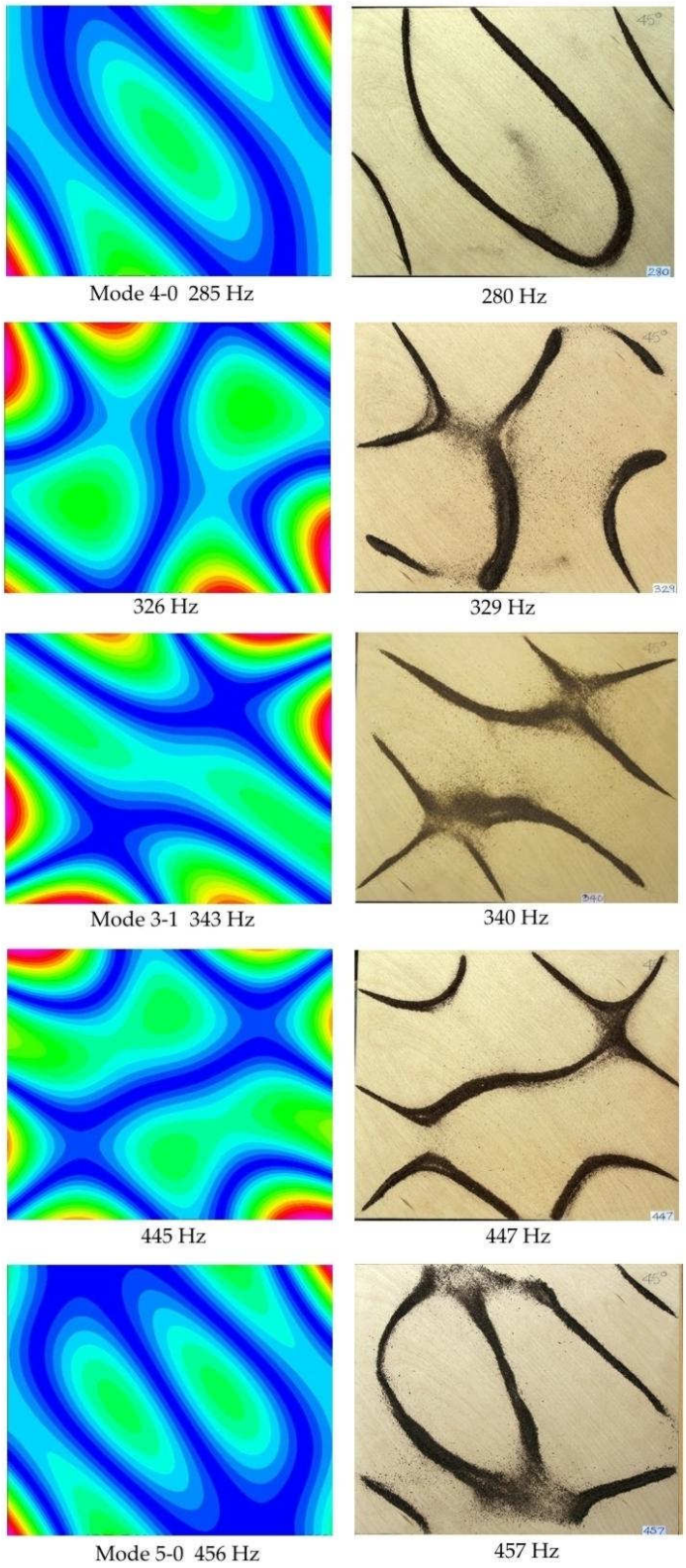

Figure 6: Birch 3-ply with grain at 45° to plate edges – medium frequency modes.

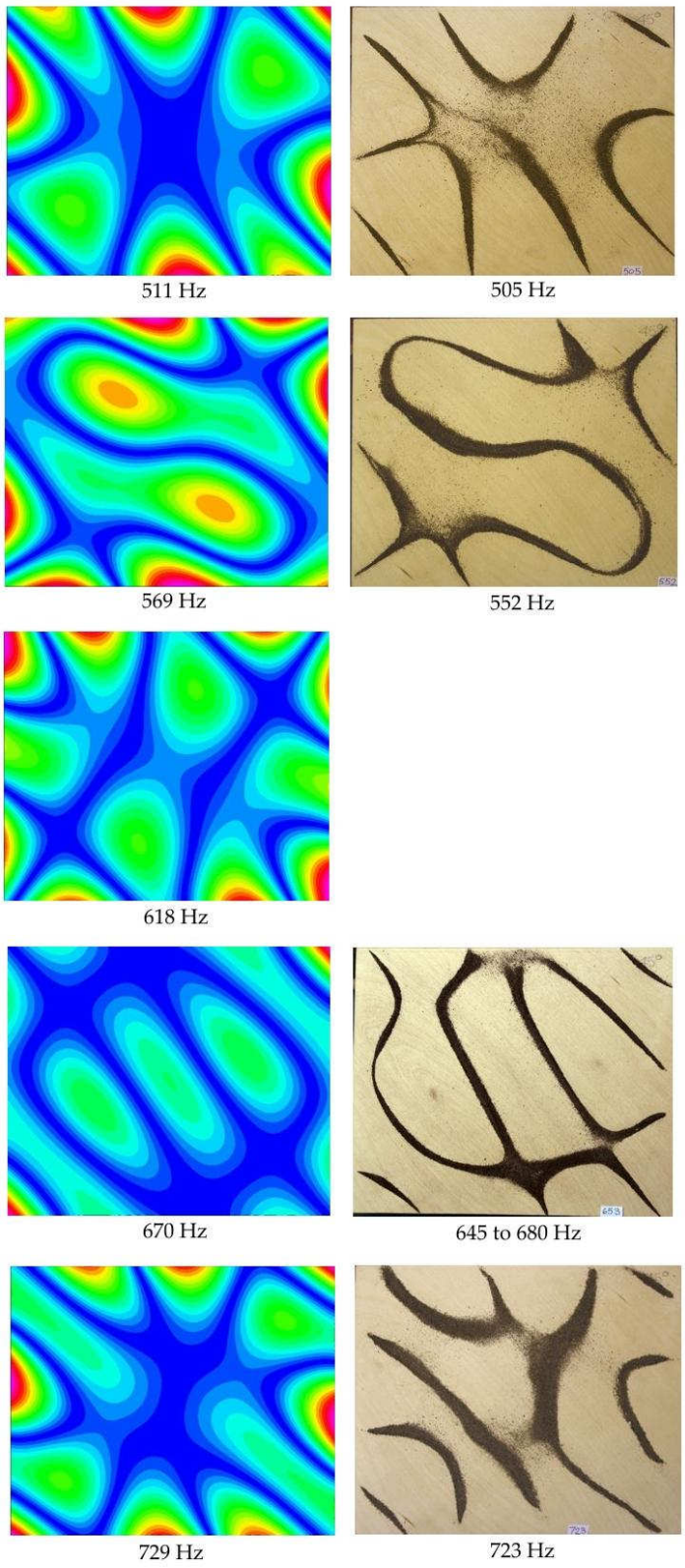

Figure 7: As previous figures at high frequencies.

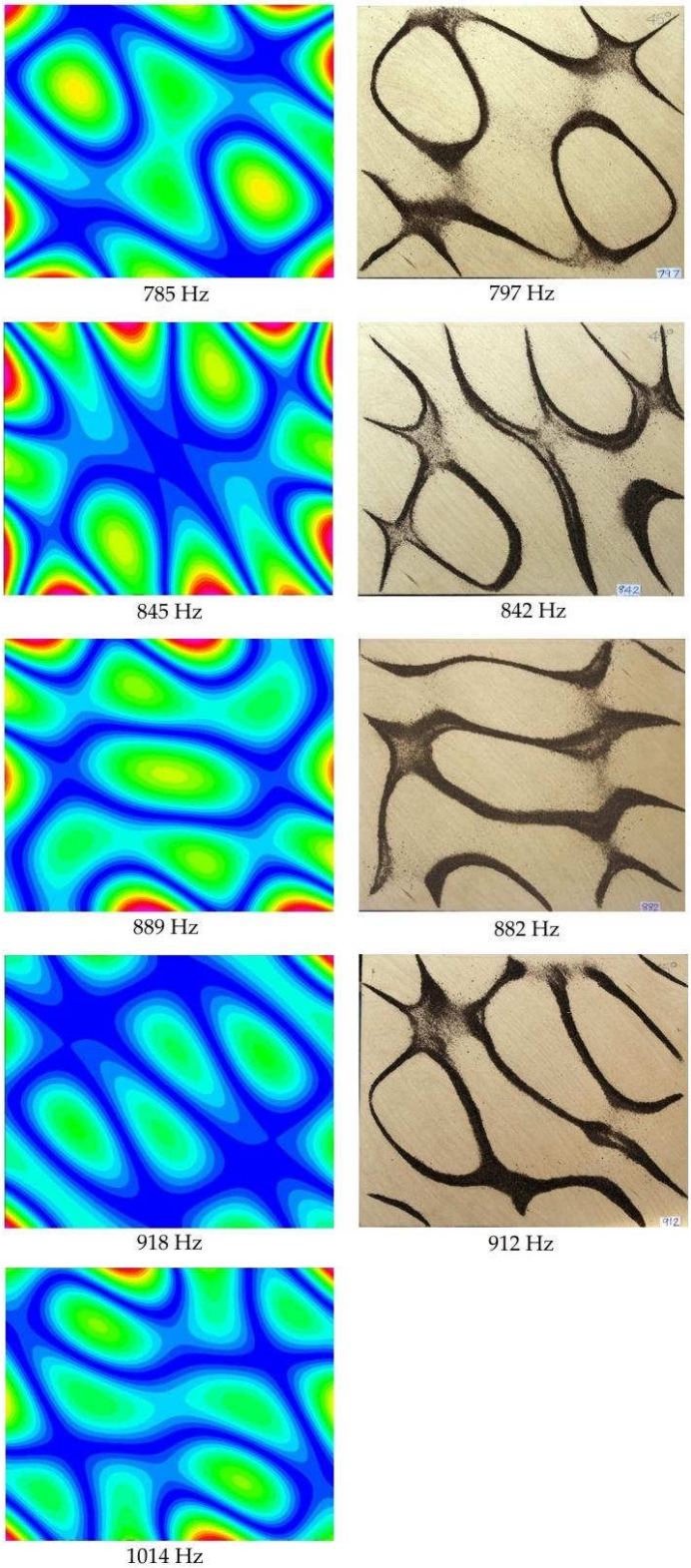

Figure 8: As previous figures at even higher frequencies.

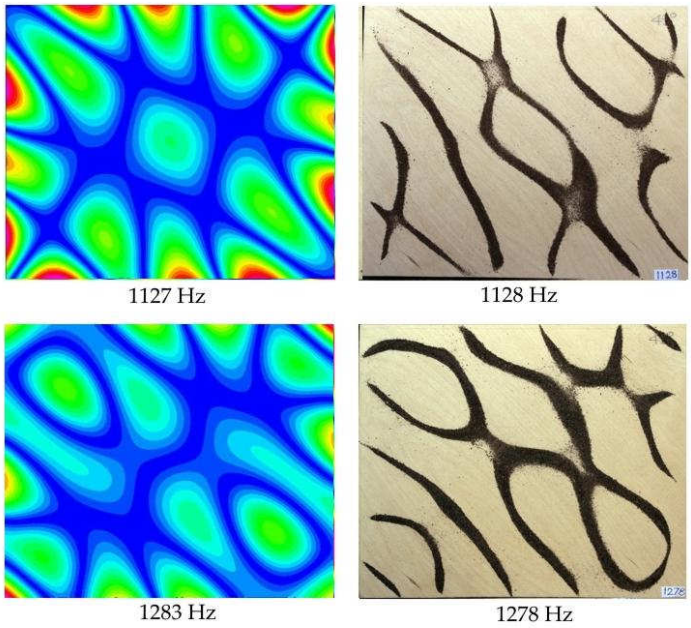

Figure 9: Two high frequency modes. These are the only two taken out of sequence.

6 Effects of wood grain direction and plate dimensions

This section uses finite element analysis with Strand7 to examine how the vibrational modes of a rectangular plywood plate vary with its side lengths, thickness and the direction of the wood grain with respect to the plate edges.

6.1 Grain angle

With an isotropic elastic plate the nodal lines are mainly parallel to the plate edges, but the dominant effect for a strongly orthotropic material is that the lines tend to follow the grain. The relative influence of edges and grain must depend on the ratio of Young's moduli E_1/E_2, the primary measure of anisotropy. In our case the ratio is $17 \cdot 9/2 \cdot 2 \approx 9$. In bulk wood the ratio typically can be 16.

In these grain rotation studies the thickness was fixed at $3 \cdot 65$ mm and the size at 250 along the surface grain, 300 mm across. I used Strand7 to model gradual rotation of the grain anticlockwise from vertical in the images to horizontal, keeping the long edge of the plate in the x (horizontal) direction. Thus the angle of the plate-shell element's local 1 axis has been incremented in $7 \cdot 5°$ steps from 90° (y direction) to 180°. Calculations are needed only for this quarter turn because the nodal pattern for $(90 - \theta)°$ is the mirror image[1] of that for $(90 + \theta)°$, and the frequency is the same. All nodal patterns except $(m - 0)$ and $(0 - n)$ become significantly distorted for rotations above about 10°. Figure 10 shows the changes in mode $(3 - 3)$. The images showing displacement contours are placed around a quadrant in positions corresponding to the grain direction. Grain rotation changes the order of several modes, and $(3 - 3)$ is a case in point; it is at position 26 in the mode table at 90°, but at 22 at 180°.

[1] It's like looking at the plate from the back.

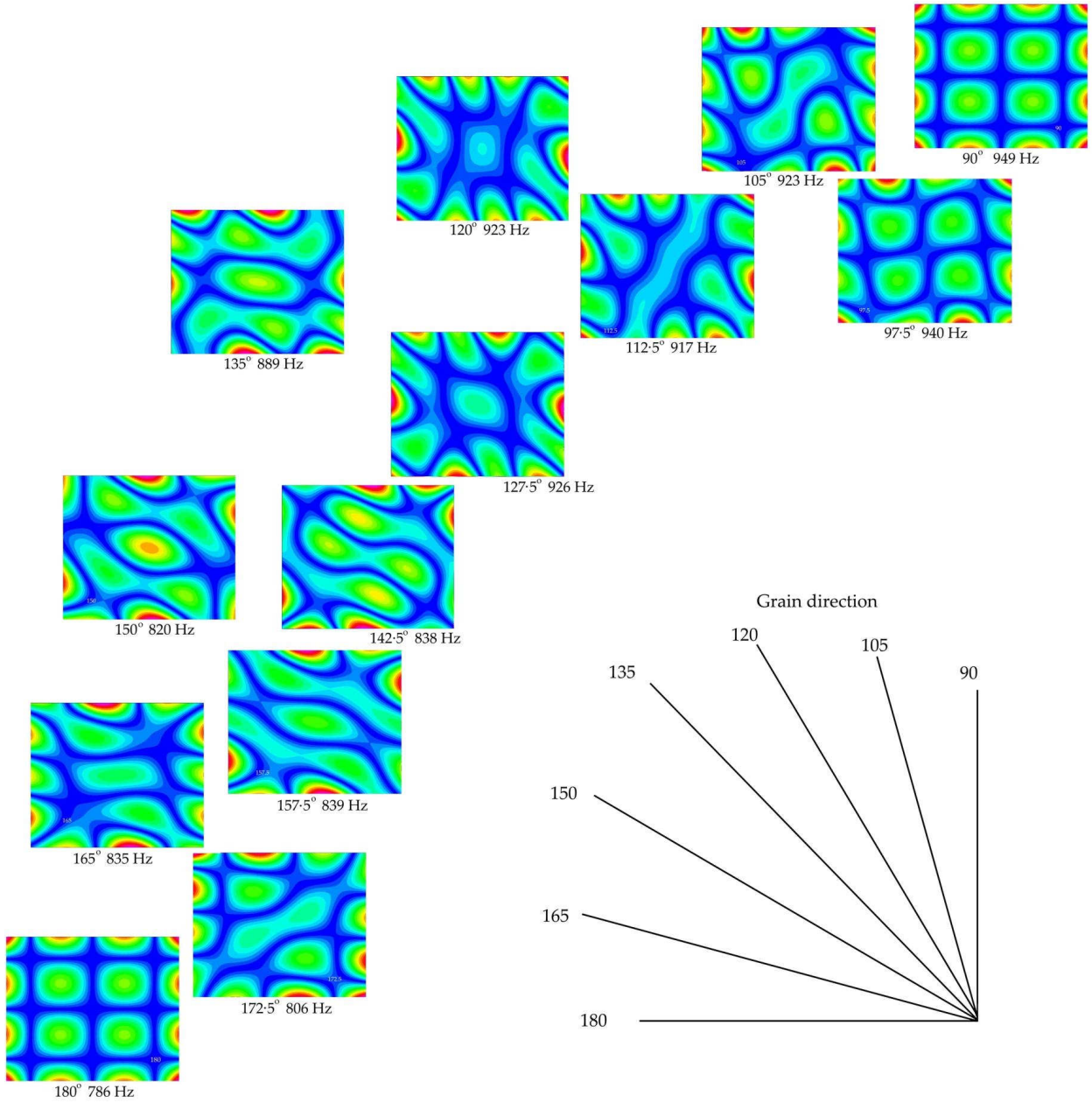

Figure 10: Variations in the displacement contours of mode $(3-3)$ as a function of wood grain direction with respect to the plate sides. Calculations using Strand7 of a birch plywood plate 250mm vertical by 300 mm horizontal. Grain angles increase by 7·5° degrees. The pictures alternate between the outer and inner quadrants.

A strange and surprising behaviour is seen with some modes in that they change their nature upon rotation. An example is shown in Figure 11 which shows mode $(2-2)$ at 90° morphing into $(1-3)$ at 180°. Clearly there is a rich structure here.

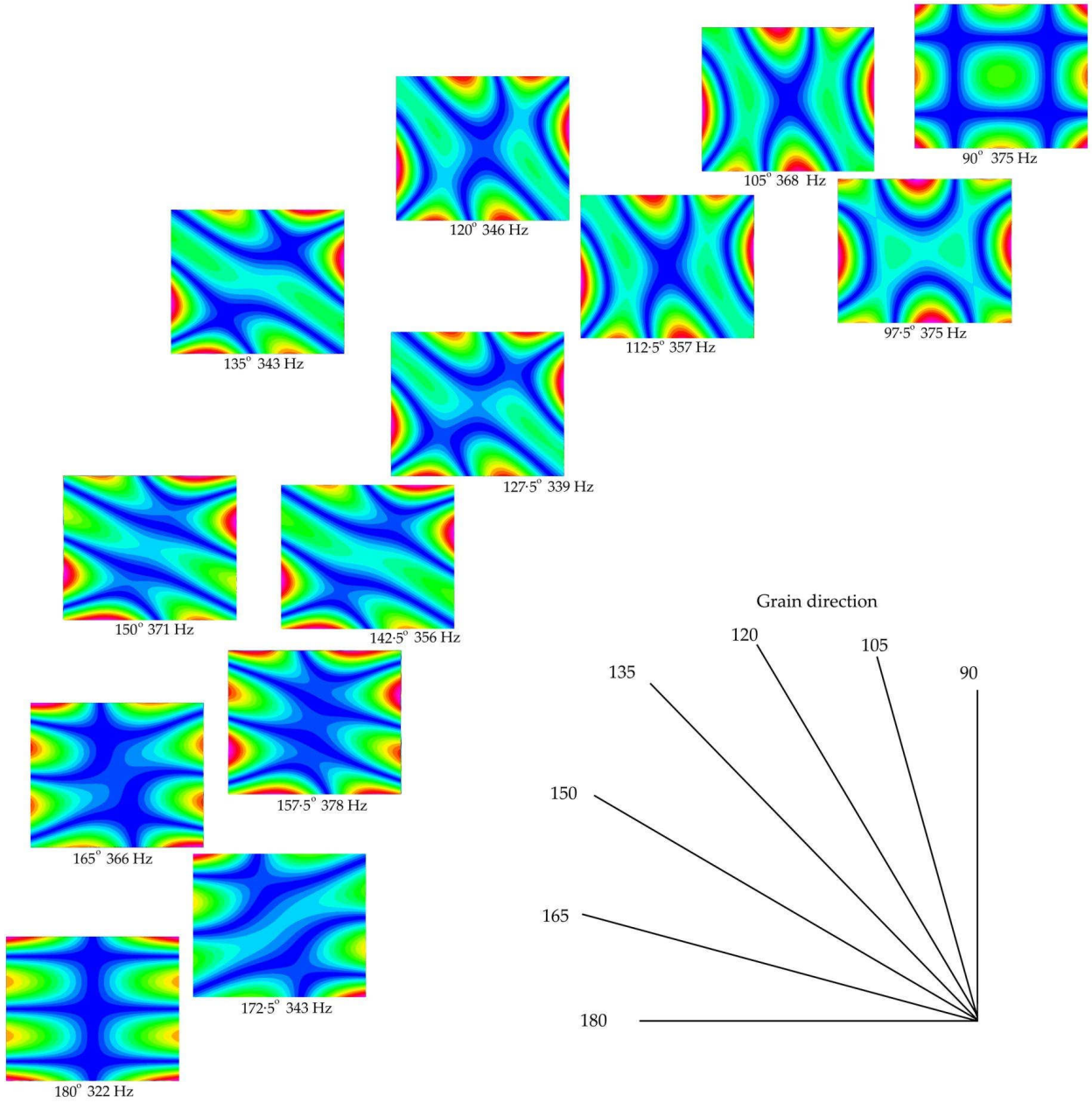

Figure 11: Morphing of mode $(2-2)$ into $(1-3)$ as the grain direction increases from 90° to 180° in the birch plywood rectangle 250 by 300 mm.

6.2 Side length and thickness

There is an analytical theory of the vibrational modes of a rectangular plate. Three important early papers are by Hearmon, Warburton and Lessa[2]. Hearmon's formula for a simply supported specially orthotropic rectangular plate is quoted in Eq 8 of my previous paper 'Modelling an orthotropic

[2]References: R.F.S. Hearmon 'The fundamental frequency of vibration of rectangular wood and plywood plates' Proc Phys Soc Lond 1946, Vol 58 p78.
G.R. Warburton 'The vibration of rectangular plate' Proc Inst Mech Eng. 1954 Vol 168 No 1 p371.
A. W. Lessa 'The free vibration of rectangular plates', J. Sound & Vibration 1973 Vol 31 No 3, p257.

material by an assemblage of isotropic components'. It reads

$$f_{m,n} \;=\; \frac{\pi}{4\sqrt{3}}\,\frac{h}{\sqrt{\rho\lambda}}\sqrt{\frac{n^4}{a^4}E_1 + 2\frac{m^2n^2}{a^2b^2}(E_1\nu_{21}+2G_{12})\lambda + \frac{m^4}{b^4}E_2}, \tag{2}$$

where the along-grain and across-grain side lengths are a and b, the thickness is h and density ρ. λ depends on Poisson's ratio and Hearmon takes $\lambda \approx 0\cdot 99$ for wood and plywood. This formula states that resonant frequencies should be proportional to thickness and, for modes $(m-0)$, $(0-n)$, inversely proportional to (side length)^2. Lessa's paper deals with all 21 cases of edge constraints on an isotropic rectangle. He expresses frequency in terms of a non-dimensional frequency parameter

$$\Omega(m,n) \;=\; fL^2\sqrt{\frac{\rho}{D}} \;\text{ where } D \;=\; \frac{Eh^3}{12(1-\nu^2)} \;\text{ making } f \;\approx\; \frac{\Omega(m,n)\,h}{2\sqrt{3}L^2}\sqrt{\frac{E}{\rho}}. \tag{3}$$

Here L is a characteristic side length and D the flexural rigidity. I have taken $\nu \approx 0$. Eq 2 states that for a specially orthotropic plate the frequencies of the $(m-0)$ and $(0-n)$ modes will be

$$f_{(m-0)} \;=\; \kappa\,\frac{m^2}{b^2}\,h\sqrt{\frac{E_2}{\rho}}, \qquad f_{(0-n)} \;=\; \kappa\,\frac{n^2}{a^2}\,h\sqrt{\frac{E_1}{\rho}}. \tag{4}$$

κ is a constant equal to $0\cdot 45$ for four simply supported edges. Our plates here are unconstrained, but we may expect the same dependence on side length and thickness.

6.2.1 Width

In a few numerical experiments with Strand7 I varied the across-grain size of the rectangular plate whilst keeping the along-grain dimension fixed at 250 mm. Table 17 lists the frequencies of the $(m-0)$ modes. According to Eq 4 the only elastic constant these depend upon is E_2, the across-grain Young's modulus.

The inverse square proportionality to width is well followed, as evidenced by the near constant values of fb^2 in the right hand panel of Table 17. The proportionality to mode order, m^2, is not so well followed – it holds approximately for the higher m values – but this is probably because we are modelling free plates, not simply supported ones for which Hearmon derived his formula. General modes with m and n both non-zero are not predicted by Eq 2 to have a simple dependence on plate size, and I have not investigated this.

	width (mm)				width (mm)			
Mode	250	300	360	432	250	300	360	432
2-0	101	70	49	34	$0\cdot 634$	$0\cdot 634$	$0\cdot 634$	$0\cdot 634$
3-0	279	194	135	94	$1\cdot 746$	$1\cdot 747$	$1\cdot 747$	$1\cdot 748$
4-0	546	380	264	183	$3\cdot 414$	$3\cdot 419$	$3\cdot 422$	$3\cdot 424$
5-0	900	627	436	303	$5\cdot 627$	$5\cdot 639$	$5\cdot 648$	$5\cdot 654$
6-0	1340	934	650	452	$8\cdot 373$	$8\cdot 402$	$8\cdot 421$	$8\cdot 435$
7-0	1862	1300	906	630	$11\cdot 64$	$11\cdot 70$	$11\cdot 74$	$11\cdot 76$
8-0			1202	838			$15\cdot 58$	$15\cdot 63$

Table 17: Frequencies of $(m-0)$ modes as functions of plate width across the grain, the along-grain dimension being fixed at 250 mm. The left panel lists the frequencies in Hz, whilst the right panel lists $f\,b^2 \;\times 10^{-7}$.

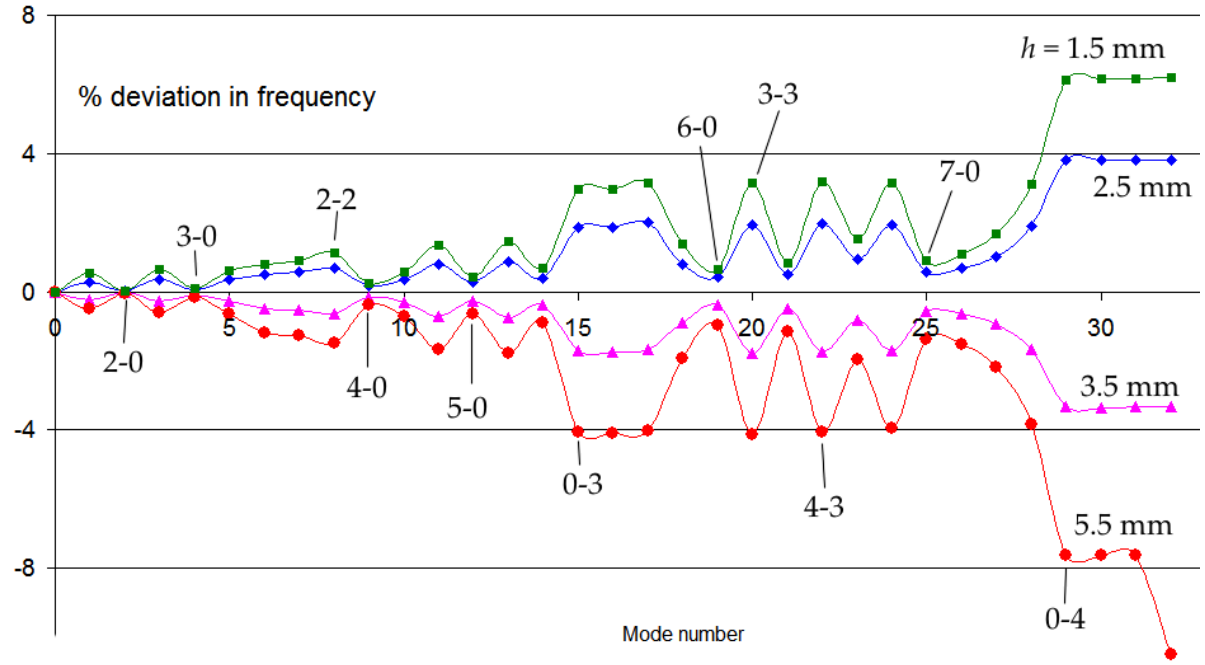

Figure 12: Deviation $\frac{3{\cdot}65\, f_h}{h\, f_{3{\cdot}65}} - 1$ expressed as a percentage for 32 modes and four thicknesses of plate. Strand7 calculations for a birch plywood plate 250mm along grain, 300 mm across. The grain orientation is 90°.

6.2.2 Thickness

The analytical theory states that $f_{(m-n)} \propto h$ for all modes. The plates modelled by Strand7 were those of §4 and §5, namely a 3-ply all-birch rectangle 250 by 300 mm. I examined grain at 90° and 135° from the x axis, where 90° means the surface grain is vertical (y direction) in the pictures. In all cases a fine FEA mesh was used, with $2{\cdot}5$ mm square quad9 elements. The elastic constants were the optimised set from §4, Eq 1. The plate with $h = 3 \cdot 65$ mm was taken as a reference, and modal frequencies calculated for other plates of $1 \cdot 5$, $2 \cdot 5$, $4 \cdot 5$ and $5 \cdot 5$ mm by changing the global finite element thickness.

These numerical simulations do indeed show, to first order, a simple scaling of all modal frequencies with thickness. For each mode we would expect the ratio

$$\frac{h}{3 \cdot 65} \text{ to equal } \frac{f_h}{f_{3{\cdot}65}}$$

meaning that

$$\frac{3 \cdot 65\, f_h}{h\, f_{3{\cdot}65}} \;=\; 1.$$

For each mode I have calculated the deviation of the actual ratio from 1. Figure 12 shows this plotted as a function of mode number for the four thicknesses. It is small – mostly less than 4%, but increasing with increasing mode number, that is, with increasing frequency.

The mode types mark in the figure show that modes $(m-0)$ generally have lower deviation from simple proportionality to h, and modes $(m-m)$ have the most. Notice also the positive deviation for thinner plates and negative for the thicker. This means that for plates thinner than the reference,

FEA predicts that a modal frequency will not be quite as low as simple proportionality to h would predict, and conversely, for a thicker plate it is not quite as high.

I find similar small deviations from $f_{(m-n)} \propto h$ when the grain direction is at 135°, roughly diagonally across the plate. I have not carried out experiments to observe the extent to which these FEA predictions hold in reality, nor have I explored to what extent they are a consequence of the mesh used. A deviation from linearity for the highest modes could perhaps be due to the material having to bend into shorter spatial wavelengths. This is turn might indicate an increasing importance of through-thickness stiffness, something that the plate-shell elements cannot adequately model. To study this further one might examine the behaviour with size different meshes and also with a fully 3D model of a thick plate at high frequency. However, because the effect is not large, I have not pursued it further.

7 Deducing elastic constants of another orthotropic material

This section considers how simply the dominant elastic constants of another type of plywood can be deduced from measurement of a few normal modes combined with a comparison with the all-birch 3-ply specimen measured more thoroughly in §4 above. For this example I have used the pink-red hardwood 3-ply listed as Specimens 3 and 4 in §2. Specimen 3 was also 250mm by 300mm, but $2 \cdot 91$ mm thick. Using the frequency spectra of tap sounds and Chladni figures, I determine that mode $(0-2)$ is at 182 Hz and mode $(0-4)$ at 985 Hz. The corresponding experimental frequencies for the birch ply are 299 Hz and 1515 Hz (see Table 13). From Eq 4 above it is easy to see that for the same mode

$$\sqrt{\frac{E_p}{E_q}} \;=\; \frac{f_p}{f_q}\,\frac{h_q}{h_p}\sqrt{\frac{\rho_p}{\rho_q}} \tag{5}$$

where p and q denote two specimens of different materials. For $(0-2)$ the calculation is

$$\sqrt{\frac{E_{new}}{E_{birch}}} \;=\; \frac{182}{299}\,\frac{3{\cdot}65}{2{\cdot}91}\sqrt{\frac{596}{700}} \;=\; 0\cdot 7045.$$

Since E_1 for birch has been deduced as being $17 \cdot 9$ GPa, E_1 for the red hardwood ply is about $8 \cdot 9$ GPa. For mode $(0-4)$ the deduced value is $10 \cdot 1$ GPa. I take $9 \cdot 5$ GPa as a working value. Notice how much less this is than for the all-birch plywood.

Moving to E_2, the new material has modes $(2-0)$, $(3-0)$ and $(4-0)$ at 83, 248 and 469 Hz respectively, compared with 70, 190 and 393 Hz for the birch ply. Since E_2 for birch is $2 \cdot 0$ GPa, by Eq 3 these frequency ratios imply that the across-grain Young's modulus E_2 of the red hardwood ply is $3 \cdot 8$, $4 \cdot 6$, and $3 \cdot 8$ GPa respectively. I have taken a working value of $4 \cdot 0$. This plywood type is closer to isotropic than the birch ply, with $E_1/E_2 \approx 2 \cdot 4$.

The shear modulus G_{12} does not follow such a simple relationship. Here $E_1\nu_{21} = E_2\nu_{12} \approx 0$ since ν_{12} was found to be effectively zero. For the same reason $\lambda = 1 - \nu_{12}\nu_{21} \approx 1$. For near-symmetric modes $(m-m)$

$$f_{m,m} \;\approx\; \kappa\,\frac{m^2 h}{\sqrt{\rho}}\sqrt{\frac{E_1}{a^4} + \frac{4G_{12}}{a^2 b^2} + \frac{E_2}{b^4}}\;. \tag{6}$$

On the assumption that ν_{12} for the new material is also close to zero, Eq 6 can be used to estimate G_{12} for the new material from the elastic constants of the birch ply by comparison of the $(2-2)$

Mode	Expt Hz	Strand7 -1 Hz	% diff	Strand7 -2 Hz	% diff
1-1		56		55	
2-0	83	86	3·3	86	4·0
2-1	140	142	1·5	140	0·2
0-2	182	188	3·4	188	3·0
1-2		219		218	
3-0	248	236	−5·0	237	−4·3
3-1		290		290	
2-2	303	306	1·1	302	−0·3
3-2		449		444	
4-0	469	461	−1·8	464	−1·1
4-1		512		512	
0-3		517		516	
1-3	532	538	1·1	535	0·6
2-3		617		612	
4-2	660	669	1·3	664	0·7
3-3		752		744	
5-0		759		764	
5-1	797	807	1·2	810	1·6
4-3		938		931	
5-2		959		955	
0-4	985	995	1·0	992	0·7
1-4		1026		1023	
2-4	1092	1080	−1·1	1074	−1·6
6-0		1129		1137	
6-1		1175		1180	
3-4		1204		1195	
4-3		1229		1222	
6-2		1316		1316	
4-4		1384		1372	

Table 18: Modal frequencies of Specimen 3, the 250 by 300 mm rectangle of red hardwood 3-ply. In the first run, labelled Strand7-1, elastic constants used were $E_1 = 9{\cdot}5$, $E_2 = 4{\cdot}0$, $G_{12} = 1{\cdot}1$, $G_{23} = 0{\cdot}5$, $G_{31} = 0 \cdot 242$ GPa, $\nu_{12} = 0$. Improved values in Strand-2 calculation were $E_1 = 9 \cdot 44$, $E_2 = 4 \cdot 06$, $G_{12} = 1 \cdot 04$, $G_{23} = 0 \cdot 51$, $G_{31} = 0 \cdot 25$ GPa, $\nu_{12} = 0$.

modes. For birch this occurs at 367 Hz, for the red hardwood ply at 303 Hz. The solution is $G_{12} \approx 1{\cdot}1$ GPa; it will be less if $\nu_{12} > 0$.

Strand7 has been run with $E_1 = 9 \cdot 5$, $E_2 = 4 \cdot 0$, $G_{12} = 1 \cdot 1$ GPa, $\nu_{12} = 0$. The modal frequencies are listed in Table 18 under heading Strand7-1, together with the few experimental values I determined. The agreement is encouraging and probably an acceptable basis for further modelling. However, we ask whether it is possible to improve the fit by adjusting the elastic parameters using Tables 4 to 9 as was done for the birch Specimen 1. These tables were created for a different material and plate thickness. The fact that ratios of frequencies were used means that changes due to thickness and density should cancel out. I have therefore only scaled the spans of the variable in proportion to the ratio of the value used for the red hardwood ply to the central value used in calculating the

tables. Thus for E_1 the span of $0{\cdot}7$ GPa has been reduced to $0{\cdot}7 \times 9{\cdot}5/16{\cdot}7$. The weightings of the various changes in elastic constants has been calculated using Excel Solver as in §5, and the slightly improved frequency predictions are listed under heading Strand7-2 in the Table 18.

To confirm the estimate of elastic constant for the red hardwood ply, I have measured and calculated normal modes for Specimen 4, a 240mm square of the plywood cut with the grain angle at 52°. Figure 13 shows eight modes determined for this plate. The corresponding FEA contours of displacement were very similar, and Table 19 compares experiment and Strand7 for these modes.

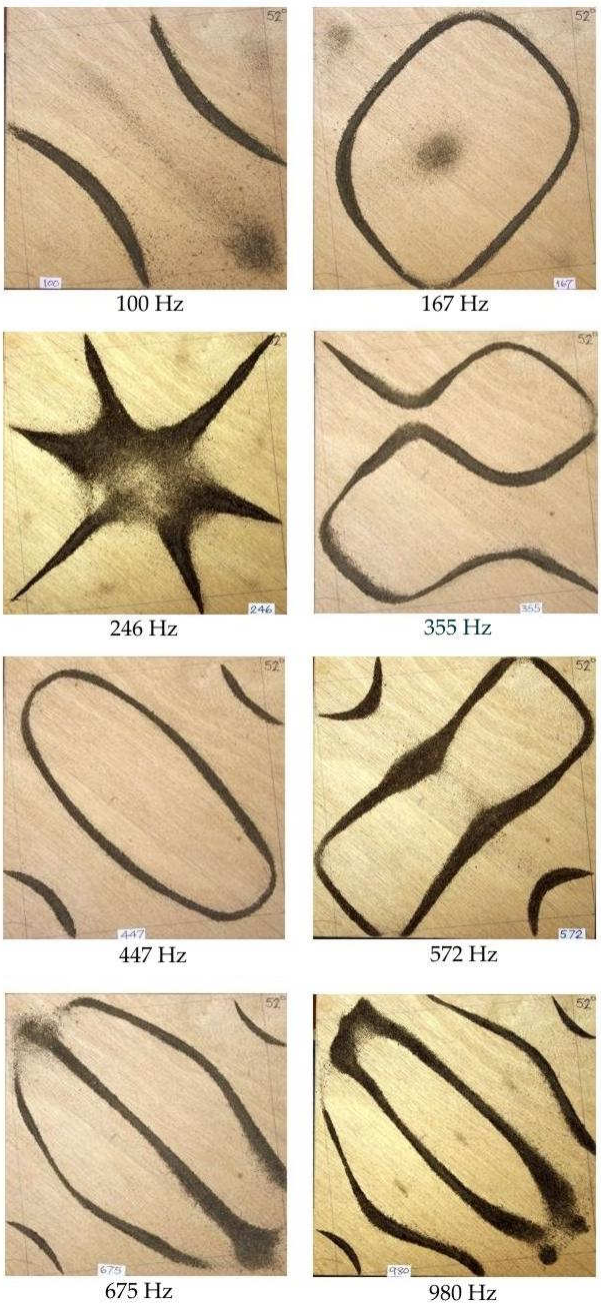

Figure 13: Chladni figures of eight resonances of Specimen 4, a red hardwood 3-ply 240 mm square with NW-SE diagonal grain (142°.

Strand7	Expt	% diff	Strand7	Expt	% diff
96	100	$-0\cdot04$	690		
114			693	675	$0\cdot027$
170	167	$0\cdot02$	754		
231			806		
267	246	$0\cdot09$	841		
358	355	$0\cdot01$	959		
420			1015	980	$0\cdot036$
431	447	$-0\cdot04$	1097		
463			1152		
578	572	$0\cdot01$	1227		

Table 19: Modal frequencies of Specimen 4, the 240 mm square of red hardwood 3-ply with diagonal grain. Comparison of measured resonant frequencies in Hz with those predicted by Strand7 using the improved input values of $E_1 = 9\cdot44$, $E_2 = 4\cdot06$, $G_{12} = 1\cdot04$, $G_{23} = 0\cdot51$, $G_{31} = 0\cdot25$ GPa, $\nu_{12} = 0$.

Overall the agreement is quite good and supports the validity of the comparative procedure outlined above for determining the elastic constants of a new, unknown material from those of a known reference specimen such as the birch 3-ply rectangle of §4.

8 Plates of irregular shape, as studied in previous article

The two final sections of my earlier article, 'Modelling an Orthotropic Material by an Assemblage of Isotropic Components', illustrated many vibrational modes for a trapezium and for a flat musical instrument plate with curved edges. Both specimens were made of $3\cdot6$ mm thick Far Eastern 3-ply from the same sheet as the top and bottom plates of a plywood 'viola' which I made, also reported on MathStudio.co.uk. Using Strand7's capability to handle orthotropic plate-shell elements, together with the machinery developed above for determining suitable elastic constants, we are now in a position to repeat the FEA modelling of these two irregular plates with 2D shell elements. I expect the results to be better than those from the quasi-orthotropic 3D model.

The first step is again to determine a consistent set of elastic constants. Here we have the complication that the reference plates of Far Eastern and birch ply were not the same size – 262 mm square compared with 250×300 mm. Scaling can be carried out as in §6.2.1 above. For both E_1 and E_2

$$\sqrt{\frac{E_p}{E_q}} \;=\; \frac{f_p}{f_q}\,\frac{h_q}{h_p}\,\frac{a_p^2}{a_q^2}\sqrt{\frac{\rho_p}{\rho_q}}. \tag{7}$$

For modulus E_1 compare modes $(0-2)$, $(0-3)$ and $(0-4)$ at 206, 566 1080 Hz for the Far Eastern ply and at 299, 802 and 1515 Hz for the birch. For $(0-2)$ the calculation is

$$\sqrt{\frac{E_{FarEast}}{E_{birch}}} \;=\; \frac{206}{299}\,\frac{3{\cdot}65}{3{\cdot}60}\,\frac{262^2}{250^2}\sqrt{\frac{680}{700}} \;=\; 0\cdot756.$$

Therefore E_1 for the Far Eastern plywood is $10\cdot2$ GPa. Remarkably, this is precisely the value measured in static bending tests as described in §5.2 of my previous article! Corresponding values for $(0-3)$ and $(0-4)$ are $10\cdot7$ and $11\cdot0$ GPa. I take $10\cdot5$ GPa as a working value.

The similar calculation for E_2 can compare modes (2–0) to (6–0). Corresponding frequencies are listed below with the consequential values of E_2. The average is $3 \cdot 79$ which I take as a working value. The value obtained in static bending tests was $3 \cdot 46$ GPa.

Far Eastern Hz	127	354	692	1142	1696
Birch Hz	70	190	393	637	945
Implied E_2 GPa	$3 \cdot 83$	$4 \cdot 04$	$3 \cdot 61$	$3 \cdot 74$	$3 \cdot 75$

There was evidence is the width studies of §6.2.1 that free plates do not follow closely the dependence on m and $n \neq m$, especially for the lower frequency modes. It is debatable whether G_{12} can be estimated from Eq 2. In fact the results are not consistent, as shown below. The highest frequency value is more likely to be correct so have taken as a working value $1 \cdot 0$ GPa, also because this is close to that of the red hardwood ply. I expect it to change at the next iteration.

Mode	(1 – 1)	(2 – 2)	(3 – 3)
Far Eastern Hz	55	334	816
Birch Hz	53	367	963
Implied G_{12} GPa	$3 \cdot 32$	$1 \cdot 75$	$1 \cdot 05$

From these working values, improved values were found as in §7 by using Tables 4 to 9 with suitable scaling. The values optimized at this second iteration are

$$E_1 = 10 \cdot 206, \quad E_2 = 3 \cdot 80, \quad G_{12} = 0 \cdot 620, \quad G_{23} = 0 \cdot 704, \quad G_{31} = 0 \cdot 246 \text{ GPa}, \quad \nu_{12} = 0 \cdot 002. \quad (8)$$

These have been used to model the vibration of two non-rectangular specimens of Far Eastern plywood studied in my previous paper.

The trapezium had been made by cutting one corner off the 262 mm reference square to leave a side 195 mm long. The agreement between Strand7 and experiment is astoundingly good, as can be seen from Table 20 and Figure 14. It is clearly much superior to the quasi-orthotropic assemblage of isotropic elements which I devised in the previous paper, in the absence of FEA software which could handle orthotropic shell-plate elements. Indeed, the Strand7 model has allowed me to identify some modes which I had found experimentally but which could not be matched with the quasi-orthotropic assemblage. Figure 14 gives a selection.

I have also modelled the curved 'musical instrument' plate. Again the agreement between FEA and experiment is pleasing. To ensure the best performance from the Strand7 model I allowed for the small variations in thickness of the plywood plate, measured with a micrometer. Accordingly, the thicknesses assigned to the FEA plate elements were adjusted in bands between $3 \cdot 45$ and 3.80 mm to match the actual plate. However, the effect on modal response was very small. I also made a new series of experimental measurements, this time using the compact acoustic exciter in place of the larger loudspeaker. These new experimental results are in good agreement with the initial ones reported in the previous paper and give me confidence that they are correct. Figures 14 and 15 show the Chladni figures in the new series of measurements (a smaller set than the previous). Next to each is the corresponding displacement contour plot from Strand7 obtained using the elastic constants of Eq 8. The third row in Figure 14 has two FEA pictures only 9 Hz apart; the theory is stating that the measured resonance at 226 Hz is actually two adjacent resonance superimposed. The reader may care to compare these images with Figures 25 to 27 in my previous article in which the quasi-orthotropic assemblage model is compared with the first series of experimental Chladni

Strand 7 Hz	Expt Hz	Strand 7 Hz	Expt Hz
61		848	846
128	127	923	921
175	172	1048	
240	245	1108	
322	313	1139	1138
347	342	1172	
375	381	1225	1226
432	433	1342	1326
560	562	1391	1374
624	646	1513	1497
688	683	1598	1606
727		1682	1726
775	773	1723	

Table 20: Comparison of resonant frequencies of the 262×195 mm trapezium of Far Eastern 3-ply as determined by Strand7 and by experiment.

figures. Values of the FEA and measured frequencies from both series of experiments are listed in Table 21.

Strand7	Old expt	New expt	Strand7	Old expt	New expt
20	25		481	500	
52	54		510	517	
73	72		558	560	
97	97	97	577	576	581
103	101	108	646	643	
124	128		682	697	694
189	200		726	716	745
219	215	226	750	737	
228	226	226	765		
254	260	260	771		
277	284		845	876	
322	331	334	864	890	
386	370	370	957	988	
418	429	427	996		
434			1008		
458	474		1017		

Table 21: Resonant frequencies of the musical instrument plate in Hz. Comparison of Strand7 calculation using optimised elastic constants with two separate series of experimental measurement.

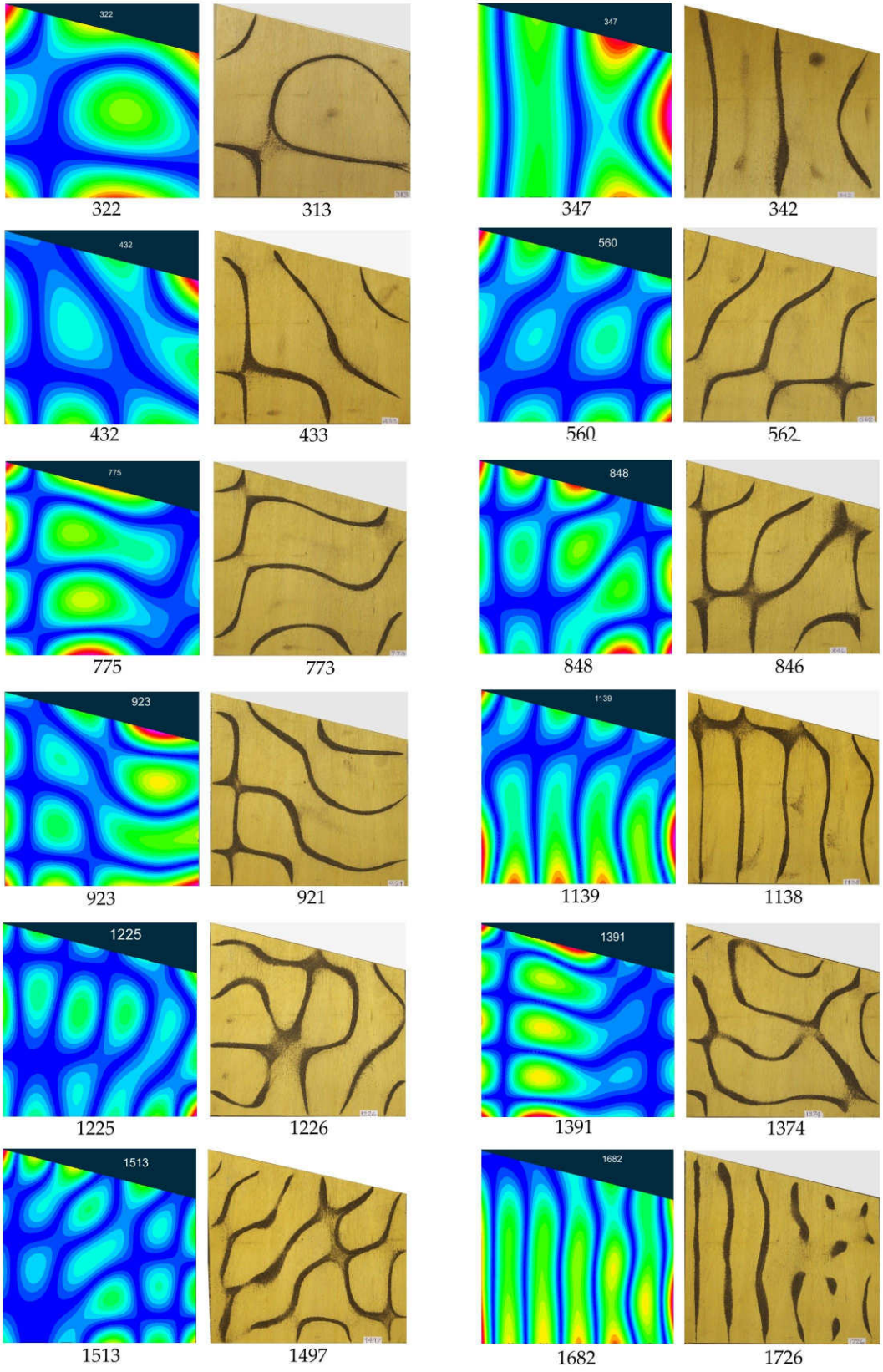

Figure 14: A selection of the vibrational modes of a trapezium of Far Eastern 3-ply. The grain lies vertically in each picture. Comparison of Strand7 model with experimental Chladni figures. Frequencies are in Hz.

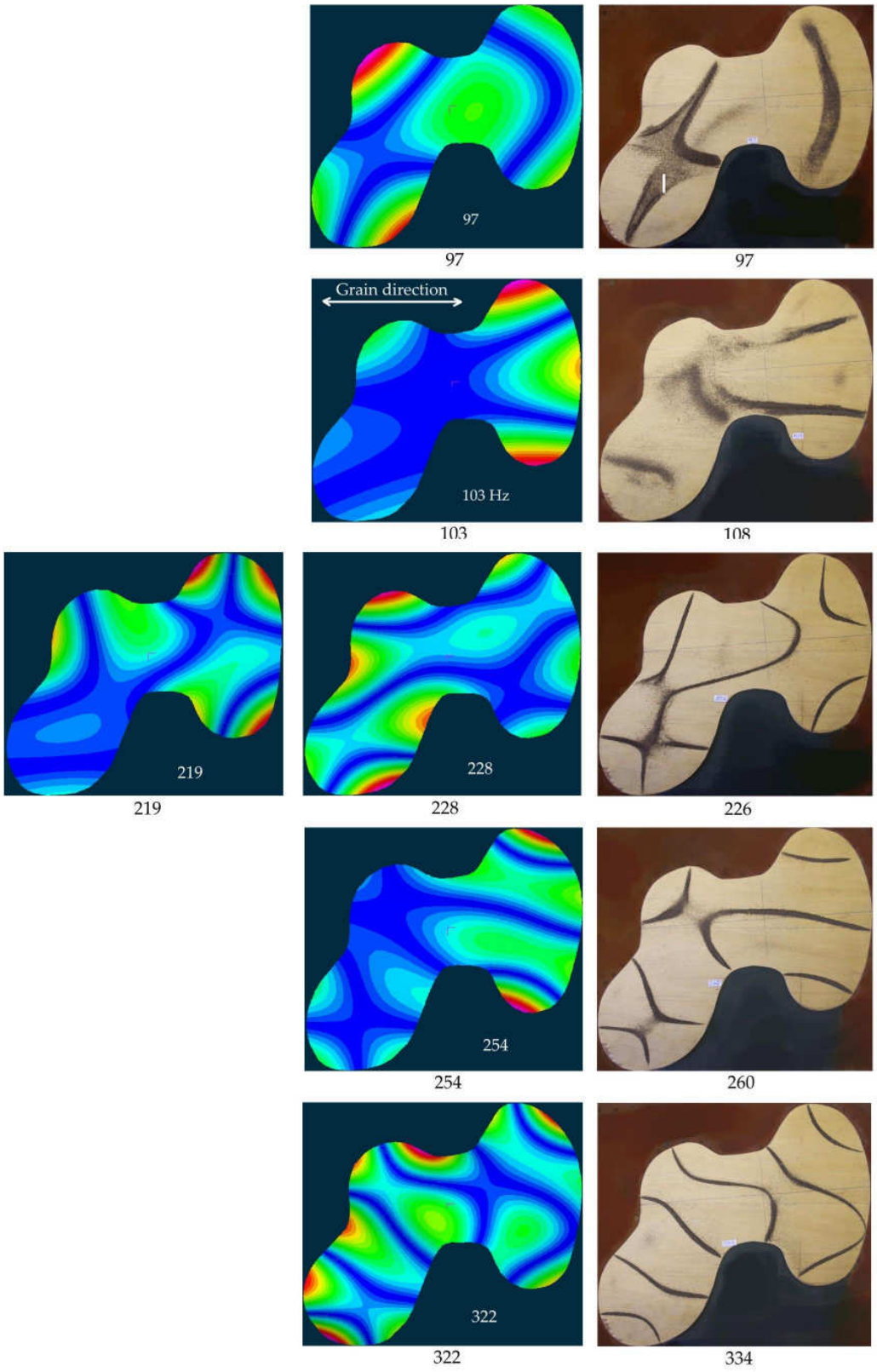

Figure 15: Strand7 model of displacement contours compared with Chladni figures for some lower modes of the flat musical instrument plate of Far Eastern 3-ply.

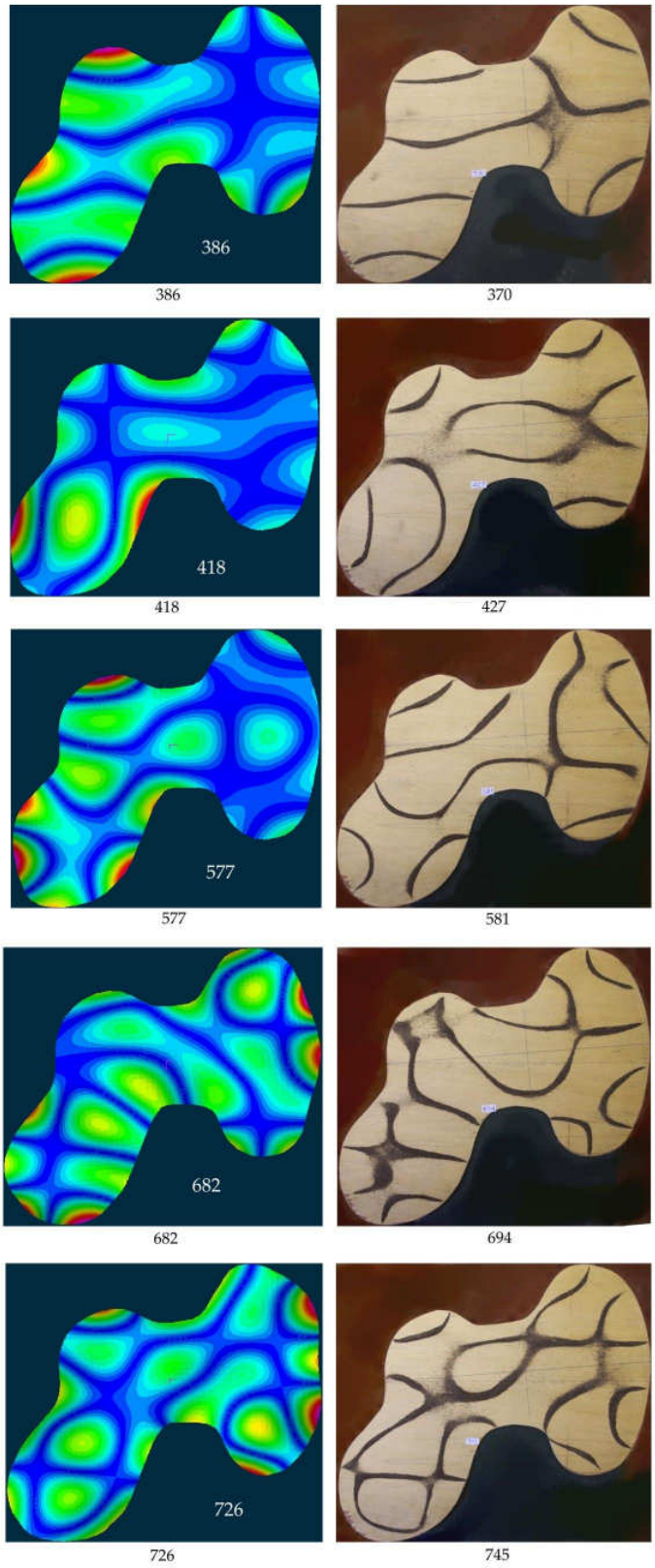

Figure 16: Strand7 model of displacement contours compared with Chladni figures for some higher modes of the musical instrument plate.

9 Summary and conclusion

This paper has examined the resonant modes of several flat plywood plates. It has compared experimental measurements, consisting of peaks in the tap sound spectra and Chladni figures at these peaks, with the eigenvalues and associated contours of out-of-plane displacement from Strand7 using 2D quad9 shell-plate elements. Strand7 requires correct elastic constants to be input, and the first half of the paper examined how these elastic constants might be determined from experimentally measured resonances. The starting point was a reference rectangular plate of all-birch 3-ply for which some elastic constants had been published in industry handbooks. FEA was used to tabulate the changes in modal frequencies due to changes in each of six elastic constants in turn (Tables 4 to 9). These tables were then used to adjust the assumed elastic constants until we had obtained a much better fit between FEA and experiment over about two dozen modes. The assumption has been made that the elastic constants which give a good fit are probably close to the true elastic constants, bearing in mind that for thin sheets only E_1, E_2 and G_{12} have a strong effect. Such a method for determining the elastic constants of plywood and similar orthotropic sheet materials is useful in itself.

When a new type of plywood is presented, it is not necessary to start the determination of elastic constants from scratch. Provided one has a rectangular specimen of the new material, §7 showed how its elastic constants can be obtained as a variation on those of the all-birch ply, making suitable scaling for plate width, thickness, density, and the frequencies of critical modes such as $(m-0)$, $(0-n)$ and (m,m).

Once an optimised set of six elastic constants has been obtained, the FEA program can predict the modal frequencies and displacement patterns of plates of various shapes, sizes and grain orientation. We have observed in Figures 5 to 11 the very strong effect of wood grain direction. This gives rise to such beautiful and complex patterns of displacement that it merits a study in itself. In all cases the agreement between theory and experiment has been very good. This gives confidence in both the FEA code plus model building, and the above procedure for determining elastic constants as input parameters.

I am most grateful to the management of Strand7 for access to an evaluation copy of their program.

John Coffey, November 2012.